

# Searching for planar signatures in WMAP

L. Raul Abramo\*

*Instituto de Física, Universidade de São Paulo, CP 66318, 05315-970, São Paulo, Brazil*

Armando Bernui†

*Instituto Nacional de Pesquisas Espaciais*

*Div. de Astrofísica, Av. dos Astronautas 1758, 12227-010 São José dos Campos – SP, Brazil*  
and

*Centro Brasileiro de Pesquisas Físicas*

*Rua Dr. Xavier Sigaud 150, 22290-180 Rio de Janeiro – RJ, Brazil*

Thiago S. Pereira‡

*Instituto de Física Teórica, UNESP - Universidade Estadual Paulista,*

*Caixa Postal 70532-2, 01156-970, São Paulo, SP, Brazil*

We search for planar deviations of statistical isotropy in the Wilkinson Microwave Anisotropy Probe (WMAP) data by applying a recently introduced angular-planar statistics both to full-sky and to masked temperature maps, including in our analysis the effect of the residual foreground contamination and systematics in the foreground removing process as sources of error. We confirm earlier findings that full-sky maps exhibit anomalies at the planar ( $l$ ) and angular ( $\ell$ ) scales ( $l, \ell$ ) = (2, 5), (4, 7), and (6, 8), which seem to be due to unremoved foregrounds since this features are present in the full-sky map but not in the masked maps. On the other hand, our test detects slightly anomalous results at the scales ( $l, \ell$ ) = (10, 8) and (2, 9) in the masked maps but not in the full-sky one, indicating that the foreground cleaning procedure (used to generate the full-sky map) could not only be creating false anomalies but also hiding existing ones. We also find a significant trace of an anomaly in the full-sky map at the scale ( $l, \ell$ ) = (10, 5), which is still present when we consider galactic cuts of 18.3% and 28.4%. As regards the quadrupole ( $\ell = 2$ ), we find a coherent over-modulation over the whole celestial sphere, for all full-sky and cut-sky maps. Overall, our results seem to indicate that current CMB maps derived from WMAP data do not show significant signs of anisotropies, as measured by our angular-planar estimator. However, we have detected a curious coherence of planar modulations at angular scales of the order of the galaxy's plane, which may be an indication of residual contaminations in the full- and cut-sky maps.

PACS numbers: 98.80.-k, 98.70.Vc, 98.80.Es

## I. INTRODUCTION

The statistical concordance model of the universe has now been established with unprecedented accuracy by the Wilkinson Microwave Anisotropy Probe (WMAP). The five year dataset release of the WMAP team [1, 2] has shown that – to a very good extent – the temperature field of the cosmic microwave background radiation (CMB) obeys a Gaussian statistic with zero mean and a variance which is the same in every direction in the sky. At the same time, several different teams [3, 4, 5, 6, 7, 8, 9, 10, 11, 12, 13] have reported the detection of statistical peculiarities in this field, mainly in the largest cosmological scales, which range from slightly to extremely unlikely within the framework of a Gaussian and statistically isotropic universe. Among these anomalies, the most conspicuous are the lack of power in the low- $\ell$  multipole sector and in the 2-point correlation function [3, 6], the alignment of the quadrupole  $\ell = 2$  and the octopole  $\ell = 3$  [5, 6, 14], and the so-called north-south asymmetry [4, 8, 9, 11, 12, 13, 15, 16, 17, 18, 19]. Several attempts to explain away these statistical features in terms of known sources of microwave radiation or peculiarities of the instrument have been proposed, but have not yet produced a compelling explanation.

If we put aside the hypotheses that these anomalies may possibly be due to some residual galactic contamination [20, 21, 22, 23] or even to a systematic data analysis effect [24, 25, 26], we inevitably end up reverse-engineering physical and/or astrophysical phenomena in order to explain these effects. Although the former explanations are important

---

\*Electronic address: abramo@fma.if.usp.br

†Electronic address: bernui@das.inpe.br

‡Electronic address: thiago@ift.unesp.br

and deserve attention on their own, the possibility that a new mechanism may explain some of the unknown CMB features is still far from being ruled out. In such a case, we have essentially two different approaches: a theoretical (bottom-up) and a phenomenological (top-down) one.

In the bottom-up approach, models for the evolution of the universe are formulated through physical principles in such a way as to account for deviations of Gaussianity and/or statistical isotropy (SI). These models usually invoke the existence of non-trivial cosmic topologies [27, 28, 29], primordial magnetic fields [30, 31, 32, 33, 34], local [35, 36, 37, 38] and global [39, 40, 41, 42] manifestations of anisotropy and even exotic models of inflation [43, 44, 45, 46, 47, 48], only to mention a few of the possibilities.

In the phenomenological top-down approach, we design statistical tools to test the robustness of temperature maps against the hypotheses of Gaussianity and SI. These approaches include statistics of multipole alignments using Maxwell's multipole vectors [6, 49, 50, 51], constructs of *a posteriori* statistics [8] and functional modifications of the two-point correlation function [52, 53, 54, 55].

One interesting feature of the top-down approach is that it can shed some light on the source of the reported anomalies without the need to invoke any specific cosmological model, but rather acting as a further guide for theorists. However, due to the intrinsic generality of this approach, it is sometimes unclear how to select the important degrees of freedom in order to construct meaningful statistical estimators. This is in fact a natural consequence of model-independent approaches, which at some stage force us to rely on our theoretical prejudices about the statistical nature of the CMB in order to construct estimators of non-Gaussianity and/or statistical anisotropy.

We can instead follow another route and let the construction of our statistics be guided primarily by what the observations tell us, rather than by what we think they should look like. Here we are primarily interested in answering: how to detect planar signatures in CMB maps? One possibility was recently proposed in [56], where the two-point correlation function is decomposed in such a way as to account for the presence of symmetry planes in temperature maps. Given that CMB experiments are confined to collecting data from inside our galactic plane, it is conceivable that we may find planar signatures in the data if foregrounds were improperly removed. Besides being observationally motivated, this approach leads naturally to both an unbiased estimator and a rotationally invariant test of statistical anisotropy, therefore alleviating the difficulties mentioned above.

In this work we employ the angular-planar power spectrum analysis introduced in [56] to search for planar signatures both in partial and full sky-coverage temperature maps, allowing for possible effects due to residual foreground contaminations. Our analysis may therefore help to shed some light in the origin of the reported anomalies and test the robustness of cleaned maps due to foreground contamination in a model-independent way.

This work is organized as follows: we start §II by reviewing the construction of the two-point correlation function, and we show how it can include planar deviations of SI. We then show that a simple chi-square analysis can be designed to detect such planarities in any theoretical cosmological model. We end that Section with a simple example of planarity which could be easily detected through our tests. In §III we discuss how the probabilities of measuring particular values of cosmological observables are usually calculated, and how this calculations can be extended to include the uncertainty inherent in this measurement. In Section §IV we explain how to include the effect of foreground contamination in our analyses, and present our results for full-sky temperature maps. After presenting the results of the analyses for masked maps in §IV B, we conclude and give some perspectives of further developments.

## II. ISOTROPIC AND ANISOTROPIC TWO-POINT CORRELATION FUNCTIONS

The starting point of our analysis is the temperature fluctuation field  $\Delta T(\hat{\mathbf{n}})$ . According to standard inflationary models, this is a random field of which we have access to one single realization. If we decompose this field in spherical harmonics:

$$\Delta T(\hat{\mathbf{n}}) = \sum_{\ell, m} a_{\ell m} Y_{\ell m}(\hat{\mathbf{n}}), \quad (1)$$

its randomness can be attributed to the multipolar coefficients  $a_{\ell m}$ , and the statistics of the field can be characterized by constructing the statistical moments of these coefficients. For simplicity, we suppose that this field is Gaussian with zero mean  $\langle \Delta T(\hat{\mathbf{n}}) \rangle = 0$ , in which case the two-point correlation function,

$$C(\hat{\mathbf{n}}_1, \hat{\mathbf{n}}_2) = \langle \Delta T(\hat{\mathbf{n}}_1) \Delta T(\hat{\mathbf{n}}_2) \rangle = \sum_{\ell_1, m_1} \sum_{\ell_2, m_2} \langle a_{\ell_1 m_1} a_{\ell_2 m_2}^* \rangle Y_{\ell_1 m_1}(\hat{\mathbf{n}}_1) Y_{\ell_2 m_2}^*(\hat{\mathbf{n}}_2), \quad (2)$$

is the only relevant statistical moment. Equivalently, the covariance matrix  $\langle a_{\ell_1 m_1} a_{\ell_2 m_2}^* \rangle$  encloses all the statistical information of the multipolar coefficients in Eq. (1). Notice that the hypothesis of Gaussianity makes no restriction

whatsoever upon the rotational properties of the two-point function  $C(\hat{\mathbf{n}}_1, \hat{\mathbf{n}}_2)$ . It is therefore perfectly legitimate to restrict our considerations to the Gaussian case when looking for deviations of SI, noting that these two questions should be clearly stated and, as much as possible, decoupled.

### A. Isotropic correlation function

The statistical counterpart of the concordance  $\Lambda$ CDM model predicts a universe which, in its linear regime, is not only Gaussian but also statistically isotropic. This means that the temperature fluctuation field (and its variance) has no privileged directions, and that the variance depends only on the angular separation of two given points in the CMB sky:

$$C(\hat{\mathbf{n}}_1 \cdot \hat{\mathbf{n}}_2) = \sum_{\ell} \frac{2\ell + 1}{4\pi} C_{\ell} P_{\ell}(\hat{\mathbf{n}}_1 \cdot \hat{\mathbf{n}}_2). \quad (3)$$

In harmonic space, rotational invariance means that the correlation function is completely diagonal:

$$\langle a_{\ell_1 m_1} a_{\ell_2 m_2}^* \rangle = C_{\ell_1} \delta_{\ell_1 \ell_2} \delta_{m_1 m_2}, \quad (4)$$

with its eigenvalues determined by the theoretical *angular power spectrum*  $C_{\ell}$ . Together, Gaussianity and SI comprise a very severe set of restrictions to the temperature field Eq. (1), and allows no expressions other than (3) and (4) to specify its properties.

### B. Planar correlation function

Deviations of SI presuppose functional deviations of the two-point function from Eq. (2). Despite the infinite possibilities that are open when one relaxes the requirement that the two-point function depends only on the separation angle  $\cos\theta = \hat{\mathbf{n}}_1 \cdot \hat{\mathbf{n}}_2$ , we should still remember that the unit vectors  $\hat{\mathbf{n}}_1$  and  $\hat{\mathbf{n}}_2$  share a common origin at the center of the CMB sphere (in other words, the center of our surface of last scattering.) One of the possibilities that do not assume isotropy is to consider  $C = C(\hat{\mathbf{n}}_1, \hat{\mathbf{n}}_1)$  [52], but in this case we would not actually be measuring correlations of two points, but rather the self-correlation of all individual points in the sky (i.e., the coincidence limit of the two-point correlation function.) Another possibility is to consider  $C = C(\hat{\mathbf{n}}_1, \hat{\mathbf{n}}_2)$  as given by expression (2), with the two vectors completely independent of each other [53]. Unfortunately this function is too general, and leads to rampant arbitrariness in the construction of statistical estimators of anisotropies, as we mentioned in §I.

A third possibility was pointed in [56]: for any pair of unit vectors in the CMB sphere, not only their angular separation is well-defined, but also the plane where they stay. That is, since these vectors are restricted to have a common origin, both their scalar and cross products are uniquely defined. This suggests that we incorporate this vectorial dependence into the two-point correlation function:

$$C(\hat{\mathbf{n}}_1, \hat{\mathbf{n}}_2) = C(\hat{\mathbf{n}}_1 \times \hat{\mathbf{n}}_2), \quad (5)$$

which can now account for both angular and planar modulations of the temperature field. Note that now vectors with the same angular separation are not necessarily correlated in the same way. This feature is what makes the functional form above suitable for detecting planar signatures in CMB sky maps, no matter if they have an astrophysical origin (as in, e.g., the galactic plane) or if they are artificially imprinted on the maps (e.g., poor masks, inhomogeneous observation function, etc.)

In practice, just as in the case of the usual (isotropic)  $C_{\ell}$ 's, it is easier to work with (5) in harmonic space. If we introduce the definition  $\mathbf{n} \equiv \hat{\mathbf{n}}_1 \times \hat{\mathbf{n}}_2 = \{\sin\vartheta, \theta, \phi\}$ , where  $\vartheta = \arccos \hat{\mathbf{n}}_1 \cdot \hat{\mathbf{n}}_2$ , we obtain the following decomposition:

$$C(\mathbf{n}) = \sum_{\ell} \sum_{l,m} \frac{2\ell + 1}{\sqrt{4\pi}} C_{\ell}^{lm} P_{\ell}(\cos\vartheta) Y_{lm}(\hat{\mathbf{n}}), \quad l \in 2\mathbb{N}, \quad (6)$$

where the restriction of the sum above to even values of  $l$  is a consequence of the reciprocity relation  $C(\hat{\mathbf{n}}_1, \hat{\mathbf{n}}_2) = C(\hat{\mathbf{n}}_2, \hat{\mathbf{n}}_1)$ . The decomposition above is equivalent to considering modulations of the function  $C_{\ell}(\hat{\mathbf{n}})$  in the sphere, where the usual angular power spectrum  $C_{\ell}$  is now given by the monopole  $C_{\ell}^{00}$ . In fact, we could have started with

this modulations rather than (6), but in such a case we would perhaps neglect the geometrical interpretation of the normal vector  $\hat{\mathbf{n}}$ , which is crucial in our analysis.

By equating Eqs. (6) and (2), it is possible to show [56] that the coefficients  $\mathcal{C}_\ell^{lm}$  are directly related to the temperature multipolar coefficients  $a_{\ell m}$ . We have that:

$$\frac{\mathcal{C}_\ell^{lm}}{\sqrt{2l+1}} = 2\pi \sum_{\ell_1, m_1} \sum_{\ell_2, m_2} \langle a_{\ell_1 m_1} a_{\ell_2 m_2} \rangle \begin{pmatrix} l & \ell_1 & \ell_2 \\ m & m_1 & m_2 \end{pmatrix} I_{\ell_1 \ell_2}^{l, \ell}, \quad (7)$$

where

$$I_{\ell_1 \ell_2}^{l, \ell} \equiv \sum_m (-1)^m \lambda_{\ell_1 m} \lambda_{\ell_2 m} \int_0^\pi d(-\cos \vartheta) P_\ell(\cos \vartheta) e^{im\vartheta} \begin{pmatrix} l & \ell_1 & \ell_2 \\ 0 & m & -m \end{pmatrix}, \quad (8)$$

with  $\lambda_{\ell m}$  a set of real coefficients resulting from the  $\vartheta$  integration and which are zero unless  $\ell + m = \text{even}$  (see the Appendix of [56] for more details). These expressions show, first, that the angular-planar multipolar coefficients  $\mathcal{C}_\ell^{lm}$  can be calculated from first principles in any theoretical model which predicts a specific form for the covariance matrix  $\langle a_{\ell_1 m_1} a_{\ell_2 m_2}^* \rangle$  like, for instance, models of anisotropic inflation [39, 40, 41, 42]. And second, given any observed temperature map, we can estimate the values of all  $\mathcal{C}_\ell^{lm}$ 's by computing the sum in Eq. (7) with the actual coefficients  $a_{\ell m}$  – see the next Subsection. Note also that the coefficients (7) are not restricted to temperature maps, and can be equally applied in the analysis of CMB polarization, large-scale structure maps or in fact any map on  $S^2$ .

### C. Statistical estimators of anisotropy

The multipolar angular-planar coefficients (7) were defined in terms of an ensemble average of the temperature multipolar coefficients  $a_{\ell m}$ . Of course, we only observe one universe, which means that the cosmic variance in the determination of the coefficients  $\mathcal{C}_\ell^{lm}$  is a severe restriction that we have to live with. This means that, if we want to evaluate the statistical properties of these coefficients, like mean values or variances, we have to build functions which can at best estimate these quantities. One obvious possibility is the following unbiased estimator:

$$\mathcal{C}_\ell^{lm} \rightarrow 2\pi\sqrt{2l+1} \sum_{\ell_1, m_1} \sum_{\ell_2, m_2} a_{\ell_1 m_1} a_{\ell_2 m_2} \begin{pmatrix} l & \ell_1 & \ell_2 \\ m & m_1 & m_2 \end{pmatrix} I_{\ell_1 \ell_2}^{l, \ell}, \quad (9)$$

which can be uniquely calculated for a given temperature map.

Following this prescription, we can now estimate the statistical moments of (9). In particular, its mean value was already calculated, and is given by  $\sqrt{2l+1}$  times the right-hand side of (7). Notice that, under the hypothesis of SI, it follows from Eqs. (9) and (4) that [56]:

$$\langle \mathcal{C}_\ell^{lm} \rangle_{\text{SI}} = C_\ell \delta_{l0} \delta_{m0}. \quad (10)$$

Conversely, if the only non-zero  $\mathcal{C}_\ell^{lm}$ 's are given by  $l = m = 0$ , then  $\mathcal{C}_\ell^{00} = C_\ell$ , and we conclude that SI is achieved if and only if the coefficients  $\mathcal{C}_\ell^{lm}$ 's are of the form (10). From now on, we will restrict our analysis to  $l \neq 0$ , since this is the first non-trivial case of planarity.

### D. A $\chi^2$ test of statistical isotropy

We have determined above, in a statistically isotropic universe, that all  $\mathcal{C}_\ell^{lm}$ 's with  $l \neq 0$  are random variables with zero mean. We can now ask, with a set of  $\mathcal{C}_\ell^{lm}$ 's at hand, how do we check whether they respect statistical isotropy – and in case they do not, which type of anisotropy they correspond to?

If we have a set of zero-mean random variables as in (10), an obvious choice would be to construct the associated chi-square test in the same way as the usual  $C_\ell$ 's are constructed as a chi-square fit from the  $a_{\ell m}$ 's. However, there is nothing which prevents us from applying this test to models where (10) *does not* hold – all that is needed is to subtract from the  $\mathcal{C}_\ell^{lm}$ 's its expectation value given by a fiducial model. Hence we can define the following (reduced) chi-square test:

$$(\chi_\nu^2)_\ell^l \equiv \frac{1}{2l+1} \sum_{m=-\ell}^{\ell} \frac{|\mathcal{C}_\ell^{lm} - \langle \mathcal{C}_\ell^{lm} \rangle|^2}{(\sigma_\ell^{lm})^2}, \quad (11)$$

where  $\langle C_\ell^{lm} \rangle$  and  $(\sigma_\ell^{lm})^2$  are respectively the expectation value and the variance of the  $C_\ell^{lm}$ 's in some particular model. Notice that, since we are summing over  $m$  in the definition of the  $(\chi_\nu^2)_\ell^l$ , our test is rotationally invariant. This is a crucial property, since we are pursuing a ‘‘blind test’’ of anisotropy where we do not know what type of directionality we are looking for.

Now that we have defined a general test of anisotropy, we need a model to be tested. As it turns out, the most successful model we have is the concordance  $\Lambda$ CDM model, for which SI holds. Under the hypothesis of SI, not only  $\langle C_\ell^{lm} \rangle$  can be easily calculated, but also the variance  $(\sigma_\ell^{lm})^2$  have a simple,  $m$ -independent, expression:

$$(\sigma_\ell^{lm})_{\text{SI}}^2 \equiv (\sigma_\ell^l)^2 = 8\pi^2 \sum_{\ell_1, \ell_2} C_{\ell_1} C_{\ell_2} \left( I_{\ell_1, \ell_2}^{l, \ell} \right)^2. \quad (12)$$

For this model, it is clear from Eqs. (10), (11), and (12) that we will have  $\langle (\chi_\nu^2)_\ell^l \rangle = 1$  as long as  $l \neq 0$ , so we define the angular-planar  $\bar{\chi}^2$  measure of the deviations of any map from SI to be:

$$(\bar{\chi}^2)_\ell^l \equiv (\chi_\nu^2)_\ell^l - 1. \quad (13)$$

If the test  $\bar{\chi}^2$  is significantly positive or negative (allowing for some variance which can be different for different maps), this will be an indication of deviations from SI.

### E. An example of planarity

Before we move on to apply (13) to actual CMB data, it is important to have some intuition on the type of planarity which could be revealed by this test. We can ask, for example, what pattern of modulations would a Gaussian and SI temperature map  $\Delta T(\hat{n})$  inherit when we apply to it a window function  $W(\hat{n})$ . Depending on the shape of this function, the resulting map

$$\Delta \bar{T}(\hat{n}) = \Delta T(\hat{n}) W(\hat{n}), \quad (14)$$

will contain planar modulations which our test (13) can easily detect. Notice, however, that this procedure is not the same as ‘cutting’ or making a ‘hole’ in the sphere  $S^2$  in order to neglect the contaminations from our galaxy with the help of a mask (as we will do in §IV B). The effect of the window function above is conceptually simpler, and corresponds to a region with enhanced/suppressed fluctuations, which naturally induces strong anisotropic correlations on  $\Delta \bar{T}$ . In particular, the resulting angular power spectrum  $\bar{C}_\ell$  will not be trivially related to the isotropic  $C_\ell$ 's, but rather it will be given by a convolution with the latter which couples different angular scales through some kernel [36, 57]. Consequently, even the angular spectrum  $\bar{C}_\ell$  would hint strongly towards anisotropy, although in this case no further information of planarity could be extracted from it.

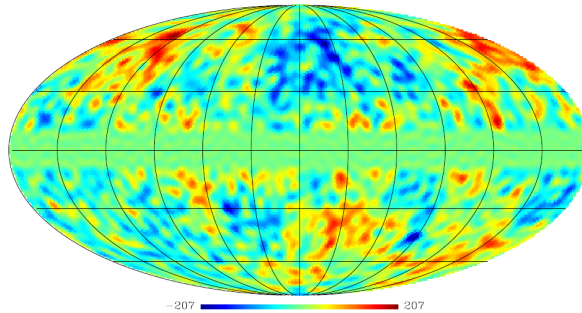


Figure 1: Temperature map with a planar signature around the equator. See the text for more details.

Having these distinctions in mind, let us take as an example a simple window function which gives zero weight for fluctuations around an equatorial strip of fixed width  $\Delta\theta$ , i.e.:

$$W(\theta) = \begin{cases} 0 & \theta \in \frac{1}{2}[\pi \pm \Delta\theta] \\ 1 & \text{otherwise.} \end{cases} \quad (15)$$

This window function introduces a disk around the equator where all points have the same temperature, as can be seen in Fig. (1). If we further decompose the function (15) in spherical harmonics and use (1), we arrive at [36]:

$$\bar{a}_{\ell m} = \sum_{\ell', m'} K_{\ell m}^{\ell' m'} a_{\ell' m'}, \quad (16)$$

with  $K_{\ell m}^{\ell' m'}$  given by

$$K_{\ell m}^{\ell' m'} = \sum_{L, M} w_{LM} \int d^2 \hat{\mathbf{n}} Y_{LM}(\hat{\mathbf{n}}) Y_{\ell' m'}(\hat{\mathbf{n}}) Y_{\ell m}^*(\hat{\mathbf{n}})$$

and where  $w_{LM}$  are the coefficients resulting from the decomposition of (15) into spherical harmonics.

Although, in principle, expression (16) could be used to explicitly evaluate both (12) and (13), the resulting expression is not clarifying. In practice it is much easier to obtain the same result by simulating these maps and applying the  $\bar{\chi}^2$  test to each one of them. Nonetheless, the relevance of Eq. (16) lies in the linear relation that is established between  $\bar{a}_{\ell m}$  and  $a_{\ell m}$ , which shows that the resulting temperature field  $\Delta\bar{T}$  will still be Gaussian, provided that  $\Delta T$  is Gaussian. In other words, in this example we have a Gaussian but anisotropic field ( $\Delta\bar{T}$ ), and therefore we will be performing a test of SI only, which is completely decoupled from the issue of Gaussianity.

Following the above prescription, we have applied the estimator (13) to  $2 \times 10^3$  maps of the form (16), with the window function chosen to cover an equatorial strip  $50^\circ$  wide; the result is shown in Fig. (2). The first thing we notice in this figure is that small planar scales (i.e.,  $\alpha \propto l^{-1} \ll 1$ , where  $\alpha$  is the angle formed by the normal of the planes that lie inside the disk and the  $z$  axis) have a roughly constant planar modulation for all the angular scales (reflected in  $\ell$ ) we tested. This is indeed what we would expect, for in this case we are probing the temperatures at points lying in circles which are nearly parallel to the equator where, by construction, the temperature is constant.

As we examine larger and larger planar scales (smaller  $l$ 's), we see that the modulations become constant only below a certain angular threshold, corresponding to those vectors that still live inside the constant temperature strip. Hence, for the planar scales  $l = 2, 4$  and  $8$ , the angular correlations level out at angular scales of approximately  $\ell \simeq 6, 10$  and  $12$ , respectively. Notice that the plateau of the  $\bar{\chi}^2$  for each  $l$ , at  $\ell \simeq 10 - 12$ , becomes smaller as  $l$  grows. This reflects the fact that the  $50^\circ$  disk induces correlations on large *planar* scales. These correlations result in a stronger signal in  $\bar{\chi}^2$  for the small *angular* scales ( $\ell \gg 1$ ) simply because for smaller angular separations there are more pairs of points that contribute coherently to  $\bar{\chi}^2$  within the disk.

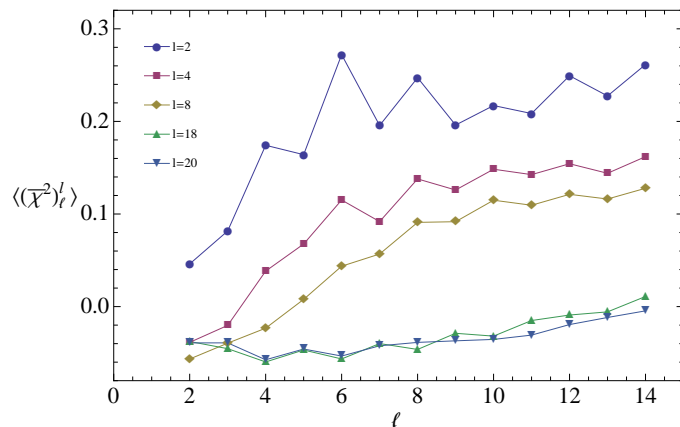


Figure 2: The angular-planar  $\bar{\chi}^2$  test averaged over  $2 \times 10^3$  maps with a planar modulation of  $\pm 25^\circ$  around the equator. The figure shows  $\langle (\bar{\chi}^2)_\ell^l \rangle$  as a function of  $\ell$  for some particular scales in the range  $l \in [2, 20]$ .

For a statistically isotropic map we would expect the  $(\bar{\chi}^2)_\ell^l$  to be randomly distributed around zero. But in the example above we see that this does not happen: there is a coherence of the  $(\bar{\chi}^2)_\ell^l$  over many  $l$ 's and  $\ell$ 's, denoting the preferred directions/planes. Hence, the main lesson from this example is that angular-planar features pointing towards statistical anisotropy can sometimes be individual anomalous values of some  $(\bar{\chi}^2)_\ell^l$ 's, which would correspond to angular-planar anomalies at particular angular scales  $\ell$  and planar scales  $l$ . However, we can also have scenarios

where the individual  $(\bar{\chi}^2)_\ell^l$ 's are not particularly anomalous, but the coherence of the test over a range of  $\ell$ 's and  $l$ 's is an indication of some preferred regions or directions. The first situation [an individual anomalous  $(\bar{\chi}^2)_\ell^l$ ] points towards a sharp anisotropic feature, whereas the second scenario [our present example, of a coherent feature in all the  $(\bar{\chi}^2)_\ell^l$ 's] points towards a wider region of anomalous correlations.

To conclude this example, we mention that although it was artificially built to illustrate the use of the angular-planar estimator, we will see in §IV B that similar modulations are found in cleaned CMB maps, even after applying the more realistic masks KQ75 and KQ85.

### III. CALCULATING PROBABILITIES

Given that our main goal is to determine how “typical” our universe is according to the test (13), we will now revisit the question of the probabilities for such tests in cosmology.

Let us suppose that we want to calculate the probability of detecting an observable inside a specific range of values, *according to a given cosmological model*. For instance, we may genuinely ask what is the probability that in a “randomly selected” Gaussian and SI universe we would measure one of the  $(\bar{\chi}^2)_\ell^l$  with a value equal or smaller (greater) than the value which is actually measured. Often, this question is analyzed as follows: suppose that the probability density function (pdf) of a given observable  $x$  in this particular model/theory is known and given by  $\mathcal{P}_{\text{th}}$ . Let us suppose further that the observation of this quantity gave us a value  $x_0$ . Then, the number:

$$P_{\leq} \equiv \int_{-\infty}^{x_0} \mathcal{P}_{\text{th}}(x) dx \quad (17)$$

denotes the probability of detecting a value  $x$  equal to or smaller than  $x_0$ , *according to this model*. The probability of having  $x > x_0$  is then given by  $P_{>} = 1 - P_{\leq}$ . However, these probabilities assume that we have measured the value  $x_0$  with infinite precision, so they say nothing about an important question that we must deal with: typically, the measurement of  $x_0$  has itself an uncertainty, which should be folded into the final probability that the observations match the theoretical expectations.

Since no measurement (of the CMB or any other physical observable) will give us a result with infinite precision, our measurements should also be regarded as random events. Therefore, in a more rigorous approach, we would have to consider  $x_0$  itself as a random variable. In the case of CMB, however, this would be only part of the whole picture, since the randomness of the measurements of  $x_0$  should also be related to the way that this data is reduced to its final form. This happens because different map cleaning procedures will lead to different values for  $x_0$ . This difference induces a variance in the data which reflects the remaining foreground contamination of the temperature maps. We will come back to this point later, after we show how to calculate probabilities when both  $x$  and  $x_0$  are random variables.

#### A. Difference of random variables

Suppose that  $x$  and  $y$  are two random variables, uniformly distributed over the range  $[0, 1]$ . What is the pdf of the new variable  $z = x - y$ ? Intuitively, we would expect this pdf to be zero for  $z = \pm 1$ , since the pairs of events  $(x, y) = (1, 0)$  and  $(0, 1)$  are the least frequent ones. By the same reasoning, we would also expect a peak around zero. The correct answer is a triangular pdf for  $z$ :

$$\mathcal{P}(z) = 1 - |z|,$$

which can be calculated by convolving the pdf's of  $x$  and  $y$ . This result can be generalized to include any type of continuous random variables [58]. This is precisely what we need, and if we define:

$$x \equiv (\bar{\chi}^2)_{\ell(\text{th})}^l, \quad y \equiv (\bar{\chi}^2)_{\ell(\text{obs})}^l, \quad z \equiv x - y,$$

then the pdf of  $z$  will be formally given by

$$\mathcal{P}(z) \equiv (\mathcal{P}_{\text{obs}} * \mathcal{P}_{\text{th}})(z) = \int_{-\infty}^{\infty} \mathcal{P}_{\text{obs}}(y) \mathcal{P}_{\text{th}}(z + y) dy = \int_{-\infty}^{\infty} \mathcal{P}_{\text{obs}}(x - z) \mathcal{P}_{\text{th}}(x) dx. \quad (18)$$

Notice that this probability density will be automatically normalized if both  $\mathcal{P}_{\text{obs}}$  and  $\mathcal{P}_{\text{th}}$  are.

According to our definitions, the probability that in a randomly selected  $\Lambda$ CDM universe we detect a value  $x \leq y$  is translated into the probability of having  $z \leq 0$ , and this is simply the area under  $\mathcal{P}(z)$  for  $z \in (-\infty, 0]$ :

$$P_{\leq} = \int_{-\infty}^0 \mathcal{P}(z) dz. \quad (19)$$

Moreover, in the ideal case where observations are made with infinite precision,  $\mathcal{P}_{\text{obs}}(y) = \delta(y - x_0)$  and we recover (17). The reader must be careful, though, not to think of (17) as a lower bound to (19), since the distributions  $\mathcal{P}_{\text{obs}}$  and  $\mathcal{P}_{\text{th}}$  are not necessarily symmetric about their mean values. In other words, a large distance from  $y$  to the *most probable* theoretical value  $x$  would not, by itself, constitute sufficient grounds to claim that this measurement of  $y$  is ‘unusual’, since its dispersion can be wide enough to render it ‘usual’ according to (19).

Finally, there remains the question of how to obtain the probability densities  $\mathcal{P}_{\text{obs}}$  and  $\mathcal{P}_{\text{th}}$ . These functions can be computed numerically, provided that the number of realizations of the random variables  $y$  and  $x$  is large enough, since in this case the histograms for these variables can be considered as piecewise constant functions which approximate the real pdf’s. For the case of the (‘theory’) variable  $x$  defined above we have run  $2 \times 10^4$  Monte Carlo simulations of Gaussian and statistically isotropic CMB maps using the  $\Lambda$ CDM best-fit  $C_\ell$ ’s provided by the WMAP team [59]. With these maps we have then constructed  $2 \times 10^4$  realizations of the variable  $x$ . This procedure was also carried using masked  $C_\ell$ ’s (corresponding to masks KQ85 and KQ75) to construct  $2 \times 10^4$  masked versions of the variable  $x$ .

The simulation of the variable  $y$ , related to the observations, is less trivial, and is intrinsically related to the way we estimate contamination from residual foregrounds. We will now detail this procedure.

#### IV. ESTIMATING THE RESIDUAL FOREGROUNDS

As mentioned before, cosmic variance is an unavoidable limitation which can be estimated by, e.g. running many different realizations of our theoretical random variable  $x$ . However, cosmic variance is far from being the sole source of uncertainties in CMB experiments. As is well-known, not only instrumental noise, but systematic errors (e.g., in the map-making process), the inhomogeneous scanning of the sky (i.e., the exposure function of the probe), or unremoved foreground emissions (even after applying a cut-sky mask) could corrupt – at distinct levels – the CMB data.

Foreground contamination, on the other hand, may have several different sources, and consequently several different ways of being included, many of which would certainly go beyond the scope of the present work. However, since different teams apply distinct procedures on the raw data in order to produce a final map, we will make the hypothesis that maps cleaned by different teams represent – to a good extent – “independent” CMB maps. We will use this hypothesis in order to estimate residual foreground contaminations by comparing these different foreground-cleaned maps.

As a matter of fact, the WMAP science team has made substantial efforts to improve the data products by minimizing the contaminating effects caused by diffuse galactic foregrounds, astrophysical point-sources, artifacts from the instruments and measurement process, and systematic errors [60, 61]. As a result, multi-frequency foreground-cleaned full-sky CMB maps were produced, named Internal Linear Combination maps, corresponding to three and five year WMAP data [1, 62]. Therefore, in order to account for the mentioned randomness, systematic, and contaminating effects of the CMB data, we include in our analyses several full-sky foreground-cleaned CMB maps, listed in Table I, which were produced using the three and five year WMAP data.

Full-sky maps	References
Hinshaw <i>et. al.</i>	[1, 62]
de Oliveira-Costa <i>et. al.</i>	[20]
Kim <i>et. al.</i>	[63]
Park <i>et. al.</i>	[64]
Delabrouille <i>et. al.</i>	[65]

Table I: Full-sky foreground cleaned CMB maps from WMAP data used in our analysis to estimate  $a_{\ell m}^{(\text{obs})}$ . Note that the reference [63] includes the analysis of maps from the three and five years WMAP releases.

The prescription we adopt to determine the distribution of the observational variable  $y$  can be equally applied either to partial or full-sky CMB maps, and is achieved as follows: we simulate Gaussian random  $a_{\ell m}$ ’s in such a way that *their central values are given by the five year ILC5 data* [1, 62], and with a variance which is estimated from



the *sample standard deviation* of all the maps listed in Table I. So, for example, suppose we have  $n$  different full-sky temperature maps at hand and we want to estimate the randomness inherent in the determination of, let's say,  $a_{32}$ . Therefore, we take:

$$\mathcal{N}(a_{32}^{\text{ILC5}}, \sigma_{32}) \rightarrow a_{32}, \quad (20)$$

with:

$$\sigma_{32} = \sqrt{\frac{1}{n-1} \sum_{i=1}^n (a_{32}^i - \bar{a}_{32})^2} \quad \text{and} \quad \bar{a}_{32} = \frac{1}{n} \sum_{i=1}^n a_{32}^i, \quad (21)$$

where  $\mathcal{N}(\mu, \sigma)$  represents a Gaussian distribution with mean  $\mu$  and standard deviation  $\sigma$ .

Our procedure may be justified by the following facts: first, the ILC5 data is undoubtedly the most accurate CMB measurement we currently have at our disposal, and for this reason it can be considered as a good approximation to the ‘‘real’’ temperature map. Secondly, as we already mentioned, by comparing different CMB maps we should have an estimate of the residual contamination which were not properly removed, and that can possibly be the source of anomalies. Note that if this contamination is indeed weak, then the sample variance above will be small, and our procedure will reduce to the standard way of calculating probabilities (see the discussion of §III). Finally, the use of a Gaussian in (20) was dictated not only by simplicity, but also by the fact that the propagation of uncertainties in physical experiments is usually assumed to follow a normal distribution.

### A. Full-sky maps

Following this procedure, we have used the full-sky maps shown in Table (I) to construct  $10^4$  Gaussian random  $a_{\ell m}$ 's, which were then used to calculate  $10^4$  realizations of  $y = (\bar{\chi}^2)_{\ell(\text{obs})}^{\ell}$ . With those variables we constructed histograms which, together with the histograms for the (full-sky) variable  $x$ , were used to calculate the final probability (19). We have restricted our analysis to the range of values  $(\ell, l) \in [2, 10]$ , since the low multipolar sector (i.e., large angular scales) is where most of the anomalies were reported. The resulting histograms and pdf's are shown in Fig. (3), and the final probabilities we obtained are show in Table (II).

$l \setminus \ell$	2	3	4	5	6	7	8	9	10
2	81.1%	73.7%	54.1%	<b>6.1%</b>	80.7%	46.4%	36.9%	47.5%	81.8%
4	74.0%	72.6%	55.0%	39.6%	74.2%	<b>93.2%</b>	51.6%	55.4%	56.3%
6	78.1%	80.7%	69.3%	52.3%	33.6%	80.0%	<b>95.0%</b>	50.3%	82.2%
8	63.5%	87.7%	18.8%	51.5%	21.4%	66.4%	31.6%	27.5%	82.3%
10	67.9%	50.0%	61.0%	<b>8.7%</b>	37.7%	59.5%	36.6%	29.2%	35.7%

Table II: Final probabilities of obtaining, in a random  $\Lambda$ CDM universe, a chi-square value smaller or equal to  $(\bar{\chi}^2)_{\ell(\text{obs})}^{\ell}$ , as given by full-sky temperature maps.

It is interesting to compare the values in Table (II) with the more naive and independent ‘error-bars’ estimate made in [56]. As anticipated there, the angular quadrupole  $\ell = 2$  does not seem anomalous under the tests we considered. The only curiosity lies in the fact that, for the scales we probed, the quantity  $(\bar{\chi}^2)_2^2$  has a probability which is always greater than 50%, meaning that the quadrupole  $\ell = 2$  has a consistently positive planar modulation.

By far, the most unlikely individual values in Table (II) are in the sectors  $(l, \ell)$  given by (2, 5), (10, 5), (4, 7) and (6, 8), and are all below a relative chance of 10% of either being too negative [(2, 5), (10, 5)] or too positive [(4, 7), (6, 8)]. Although these modulations do not extend to a significant range of  $l$  values, it is possible that these sectors are contaminated by foreground residuals. If this is the case, then these anomalies should not be present in masked temperature maps. Conversely, if these are the only anomalies present in CMB data, then the next cut-sky maps analyses should not reveal other extreme probability values (i.e., lower than 10% or higher than 90%). We will analyze these questions in more detail in the next Section.

But before we turn to the masked maps, it is important to realize that not only the individual values of  $(\bar{\chi}^2)_{\ell}^{\ell}$  are relevant: their coherence over a range of angular or planar momenta also carries interesting information. So, for example, a set of  $(\bar{\chi}^2)_{\ell}^{\ell}$ 's which are all individually within the cosmic variance bounds, but which are all positive

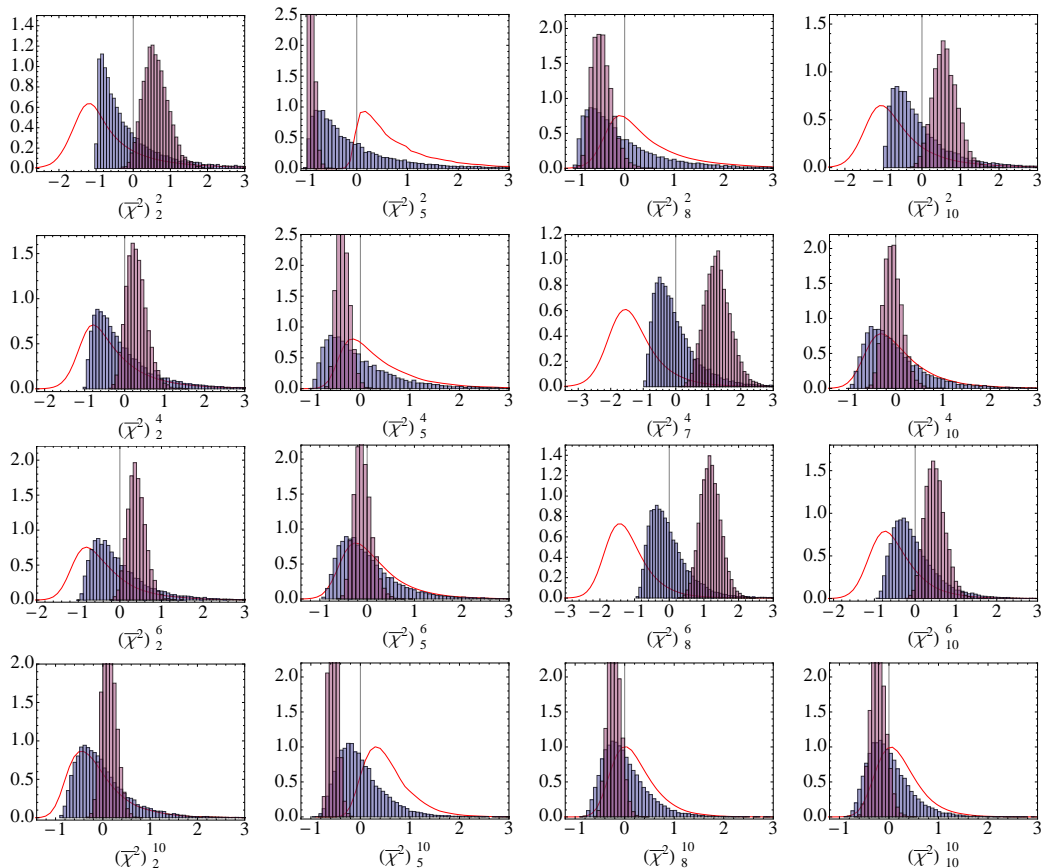


Figure 3: Full-sky maps pdf's for  $(\bar{\chi}^2)_{\ell(\text{th})}^l$  (blue histograms),  $(\bar{\chi}^2)_{\ell(\text{obs})}^l$  (purple histograms) and for the difference  $(\bar{\chi}^2)_{\ell(\text{th})}^l - (\bar{\chi}^2)_{\ell(\text{obs})}^l$  (solid red line). We show only a few representative figures since the remaining ones are qualitatively the same. The final probabilities are shown in Table (II) and correspond to the area under the solid curve from  $-\infty$  to 0. All pdf's are normalized to 1.

(or negative) can be an indication of an excess (or lack) of modulation. In fact, as we have shown in §IIE, if one suppresses a Gaussian and isotropic map only over a thick disk between fixed latitudes, the effect is to boost/depress the modulations compared with the isotropic case, over a large range of  $l$ 's and  $\ell$ 's. The  $l$ 's and  $\ell$ 's which are most affected are the ones corresponding to the angular scales subtended by the disk, but all momenta  $l$  and  $\ell$  of the angular-planar spectra are affected, with the net effect that they gain a positive/negative bias.

This type of coherent behavior (an apparent bias) is in fact exactly what we observe in the following cases:  $(\bar{\chi}^2)_2^l$ ,  $(\bar{\chi}^2)_3^l$  and, to a lesser extent,  $(\bar{\chi}^2)_\ell^l$  – see Table II. The angular quadrupole  $\ell = 2$ , as well as the angular octopole  $\ell = 3$ , have all positive planar spectra (for all values of  $l$  which we were able to compute), indicated by probabilities larger than 50%. The planar hexadecupole  $l = 4$  also has 8 out of 9 angular spectra assuming positive values (only  $\ell = 5$  is negative). Again, we stress that the data analyzed in this Section relates to the full-sky maps, which are certainly still affected by residual galactic foregrounds, so it is important that we only draw conclusions after looking into the same results for the cut-sky (masked) maps – the subject of our next Section.

## B. Masked maps

Our objective here, for completeness, is to perform the search for planar signatures in foreground-cleaned masked CMB maps. For this we will compare the masked (observational) variables  $y$  with the masked (theoretical) variables  $x$ . Following the WMAP science team recommendation to reject residual foregrounds contamination in temperature analyses of the CMB data we shall use the KQ85 mask, which cuts 18.3% of the sky data. Additionally, we also test the sensitivity of our results under the effect of the more severe KQ75 mask, which represents a cut-sky of 28.4%. Our final results for such analyses are shown in Tables (III) and (IV) and Figs. (4) and (5).

Regarding the results of our analysis, we start by noting that the sectors  $(l, \ell) = (2, 5)$ ,  $(4, 7)$  and  $(6, 8)$ , which have relative probabilities of 6.1%, 6.8% and 5% in the full-sky maps case, have now relative lower bounds given by 23.1%, 20.9% and 11.1% for the mask KQ85 and 43.7%, 21.5%, and 14.6% for the mask KQ75, respectively. This reinforces an earlier claim that the planar anomalies detected in these scales are a consequence of residual foreground contaminations in the full-sky maps [56].

On the other hand, the angular scale  $\ell = 5$  at  $l = 10$  is still below the 10% threshold, even when we apply the severe KQ75 mask. Curiously, this scale was also reported by other groups [6, 66] as being anomalously spherical. The 10% level we found here corroborates this outcome, since a very negative value of  $(\bar{\chi}^2)_\ell^l$  indicates a lack of planar modulations.

The reader may have noticed that the sectors  $(10, 8)$  and  $(2, 9)$  in the KQ75 case are also below the 10% threshold. We argue that these results could be showing that the foreground cleaning procedures (used to generate the full-sky CMB map) may not only create false anomalies, but also hide others, in this case the sticky points at the angular scales  $\ell = 8, 9$ , which became clear only after the application of the recommended cut-sky mask. Nevertheless, whether these anomalies are real or caused by some systematic error in the map-making process, they suggest that further analyses are welcome.

$l \setminus \ell$	2	3	4	5	6	7	8	9	10
2	57.8%	60.2%	47.0%	23.1%	51.1%	60.7%	58.8%	15.5%	84.9%
4	81.6%	75.7%	66.1%	34.5%	52.1%	79.1%	76.1%	61.9%	50.3%
6	75.2%	88.7%	54.3%	46.2%	31.6%	56.3%	88.9%	16.9%	88.4%
8	82.2%	77.6%	20.3%	43.1%	20.9%	47.0%	37.1%	29.7%	82.0%
10	65.2%	38.1%	52.8%	<b>3.2%</b>	60.8%	60.4%	36.7%	32.5%	68.9%

Table III: Final probabilities of detecting, in a random  $\Lambda$ CDM universe with a galactic cut of 18.3% (KQ85 mask), a chi-square value smaller or equal to  $(\bar{\chi}^2)_{\ell(\text{obs})}^l$ .

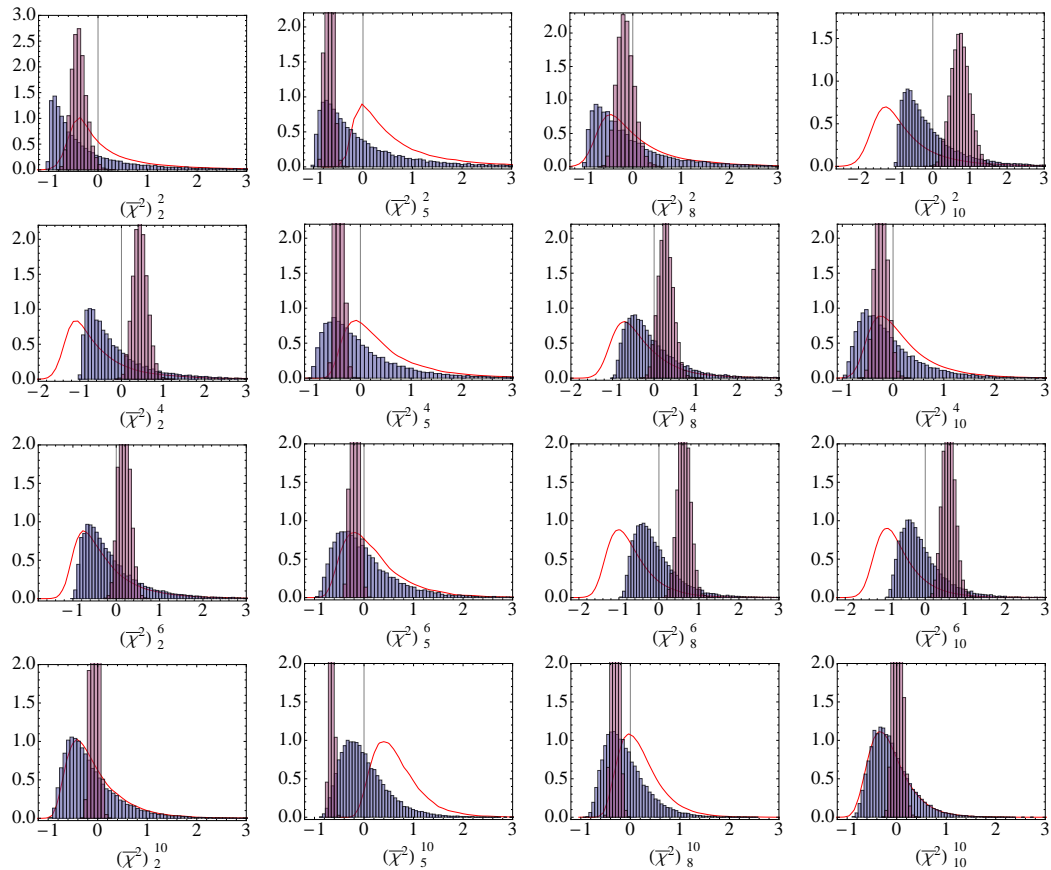


Figure 4: Pdf's for  $(\bar{\chi}^2)_{\ell(\text{th})}^l$  (blue histograms),  $(\bar{\chi}^2)_{\ell(\text{obs})}^l$  (purple histograms) and for the difference  $(\bar{\chi}^2)_{\ell(\text{th})}^l - (\bar{\chi}^2)_{\ell(\text{obs})}^l$  (solid red line) for maps with mask KQ85. Again, we only show some representative figures for simplicity. The final probabilities are shown in Table (III).

Finally, we turn to the coherence of the angular-planar spectra  $(\bar{\chi}^2)_{\ell}^l$  over a range of  $l$ 's and  $\ell$ 's. First, notice that the angular quadrupole  $\ell = 2$  shows again excessively positive modulations both for the KQ85 and KQ75 masks –although for the KQ75 case the planar  $l = 2$  spectrum is marginally negative. The angular octopole  $\ell = 3$  is now only slightly anomalous: four out of the five spectra we computed turn out to be positive. The other case we discussed in the full-sky maps,  $l = 4$ , is still marginal: eight out of the nine spectra assume positive values.

However, the most prominent feature that appears more clearly in the cut-sky maps is that  $\ell = 5$  has an anomalous coherence, with mostly rather negative values. In fact,  $\ell = 7$  and  $\ell = 10$  also show a high degree of uniformity with larger-than-expected modulations. As we showed in a previous Section, this type of coherence is the hallmark of a preferred plane (actually, of a disk-like region around a preferred plane.) Although we have not produced a test for this coherent signal, we believe our findings show that these angular scales deserve further investigation, and, given that they appear at approximately the angular size of the galactic cut, the coherence in  $(\bar{\chi}^2)_{\ell}^l$  could be pointing towards residual contaminations in the cut-sky maps.

$l \setminus \ell$	2	3	4	5	6	7	8	9	10
2	47.6%	41.4%	44.3%	43.7%	51.4%	73.3%	55.9%	<b>7.3%</b>	72.2%
4	78.1%	73.1%	54.5%	39.7%	50.0%	78.5%	62.7%	74.5%	62.9%
6	60.2%	86.1%	61.2%	35.9%	25.0%	58.6%	85.4%	10.6%	75.0%
8	86.6%	70.5%	33.4%	52.0%	35.4%	72.7%	24.6%	64.1%	77.5%
10	57.5%	64.7%	43.6%	<b>4.6%</b>	67.6%	58.8%	<b>6.6%</b>	38.3%	52.2%

Table IV: Final probabilities of detecting, in a random  $\Lambda$ CDM universe with a galactic cut of 28.4% (KQ75 mask), a chi-square value smaller or equal to  $(\bar{\chi}^2)_{\ell(\text{obs})}^l$ .

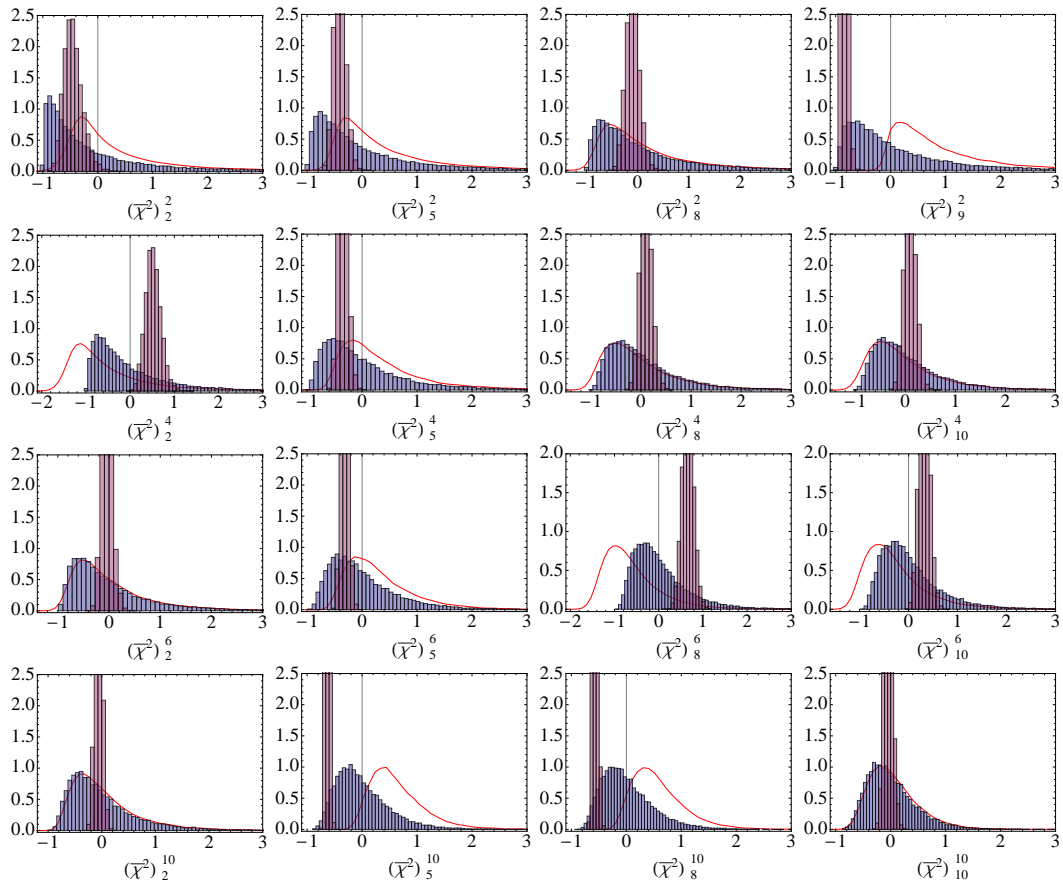


Figure 5: Pdf's for  $(\bar{\chi}^2)_{\ell(\text{th})}^l$  (blue histograms),  $(\bar{\chi}^2)_{\ell(\text{obs})}^l$  (purple histograms) and for the difference  $(\bar{\chi}^2)_{\ell(\text{th})}^l - (\bar{\chi}^2)_{\ell(\text{obs})}^l$  (solid red line) for maps with mask KQ75. The final probabilities are shown in Table (IV).

## V. CONCLUSIONS

We have used a top-down approach to search for deviations of statistical isotropy in the WMAP data by means of the recently introduced  $\chi^2$  test for angular-planar modulations [56].

These tools, designed to account for the presence of physical/astrophysical planes in temperature maps, can unveil any kind of planar modulations in these maps in a completely model-independent way. Furthermore, since improper subtraction of foreground contamination around the galactic plane in CMB data may lead to planar signatures, the angular-planar statistic can be a valuable tool to test the robustness of map cleaning procedures. Due to its generality and model independence, the angular-planar power spectrum  $C_\ell^{lm}$  can be applied to any given temperature map—in fact, to any map whatsoever on the sphere  $S^2$ .

In this work we have applied this estimator to three classes of WMAP maps, namely, full-sky cleaned maps and masked cleaned maps due to the application of the WMAP 5-year KQ85 and KQ75 masks. We have included in our analyses an estimation of residual foreground contamination as well as an assessment of these types of errors in the final probabilities we calculated.

The analysis with full-sky maps have shown that the angular quadrupole  $\ell = 2$  has a consistently positive planar modulation throughout the range  $l \in [2, 10]$ . This systematic positivity could be an indication of a planar signature around  $\ell = 2$ , although we would need to consider a wider planar range to confirm this suspicion. On the other hand, we have found slightly anomalous values in the angular-planar  $(l, \ell)$  sectors  $(2, 5)$ ,  $(10, 5)$ ,  $(4, 7)$  and  $(6, 8)$ , with relative probabilities of 6.1%, 8.7%, 6.8% and 5%, respectively.

As argued in [56], these anomalies are not drastically low, and can be attributed to residual foreground contamination. Our analyses with masked maps confirms that this is indeed the case for the sectors  $(l, \ell) = (2, 5)$ ,  $(4, 7)$  and  $(6, 8)$ . While in the full-sky map analysis the lower bound for the above probabilities was of  $\sim 5\%$ , in the case with the mask KQ75 this bound was raised to 14.6%. This confirms earlier claims that foreground contamination may be an important issue when analyzing CMB anomalies, and that more reliable results should always be based in masked

maps analyses.

On the other hand, we have found a significant trace of anomaly in the sector  $(l, \ell) = (10, 5)$ . This value seems to be robust under the effect of the two masks we used – lower values being allowed with only 4.6% of chance in the case of the mask KQ75. Curiously, the angular scale  $\ell = 5$  was reported to be highly spherical by other groups [6, 66], while we have found that it has a very low planar modulation. However, the multipole vectors used in that analysis do not represent physical directions in a straightforward manner, so the term “spherical” in this context should be used carefully. Nonetheless, it is interesting that this scale has conspicuously appeared as anomalous in two rather different tests of planarity.

Perhaps the strongest indication of a possible anisotropy in the CMB maps was provided by the coherence of our  $\bar{\chi}^2$  test on the angular scales corresponding to  $\ell = 5, 7$  and 10. As we showed, this uniformity of mostly negative or positive values of  $\bar{\chi}^2$  is equivalent to the signal left by a preferred plane (actually, a preferred disk with some thickness related to  $l$ ). This may point towards contaminations in the masked maps which were left over from the foreground-cleaning process, although further work will be necessary to confirm this suspicion.

As a final comment, we would like to mention that the approach we used to calculate our final probabilities, namely, the convolution of the observational and theoretical probability densities, is more rigorous than the widely used method of just computing the area under the theoretical probability density function. This approach generalizes the former, and implements in a natural way the uncertainty inherent in CMB observations, which in turn have a non-trivial impact in the final probabilities predicted by a specific cosmological model.

In what regards prospects for further developments, we would like to point out that the tests used here are completely general and have a wide range of applications, among which we can mention polarization maps, tests of non-Gaussianity and even stacked maps of cosmic structure, like the galaxy cluster catalog 2Mass [67].

### Acknowledgments

We would like to thank Marcelo J. Rebouças for useful suggestions during the early stages of this work. AB was supported by the Brazilian agency CNPq (309388/2008-2). Some of the results in this paper have been derived using the HEALPix package [68]. We are also grateful for the use of the Legacy Archive for Microwave Background Data Analysis (LAMBDA) [1]. This work was supported by Fundação de Amparo à pesquisa do Estado de São Paulo (Fapesp) and by CNPq.

- 
- [1] WMAP, G. Hinshaw *et al.*, *Astrophys. J. Suppl.* **180**, 225 (2009), 0803.0732.
  - [2] WMAP, E. Komatsu *et al.*, *Astrophys. J. Suppl.* **180**, 330 (2009), 0803.0547.
  - [3] A. de Oliveira-Costa, M. Tegmark, M. Zaldarriaga, and A. Hamilton, *Phys. Rev.* **D69**, 063516 (2004), astro-ph/0307282.
  - [4] H. K. Eriksen, F. K. Hansen, A. J. Banday, K. M. Gorski, and P. B. Lilje, *Astrophys. J.* **605**, 14 (2004), astro-ph/0307507.
  - [5] D. J. Schwarz, G. D. Starkman, D. Huterer, and C. J. Copi, *Phys. Rev. Lett.* **93**, 221301 (2004), astro-ph/0403353.
  - [6] C. J. Copi, D. Huterer, D. J. Schwarz, and G. D. Starkman, *Mon. Not. Roy. Astron. Soc.* **367**, 79 (2006), astro-ph/0508047.
  - [7] K. Land and J. Magueijo, *Phys. Rev. Lett.* **95**, 071301 (2005), astro-ph/0502237.
  - [8] A. Bernui, B. Mota, M. J. Rebouças, and R. Tavakol, *Astron. Astrophys.* **464**, 479 (2007), astro-ph/0511666.
  - [9] H. K. Eriksen, A. J. Banday, K. M. Gorski, F. K. Hansen, and P. B. Lilje, *Astrophys. J.* **660**, L81 (2007), astro-ph/0701089.
  - [10] B. Lew, *JCAP* **0809**, 023 (2008), 0808.2867.
  - [11] P. K. Samal, R. Saha, P. Jain, and J. P. Ralston, *Mon. Not. Roy. Astron. Soc.* **385**, 1718 (2008), 0708.2816.
  - [12] P. K. Samal, R. Saha, P. Jain, and J. P. Ralston, (2008), 0811.1639.
  - [13] A. Bernui, *Phys. Rev.* **D78**, 063531 (2008), 0809.0934.
  - [14] A. Gruppuso and C. Burigana, (2009), 0907.1949.
  - [15] A. Bernui, T. Villela, C. A. Wuensche, R. Leonardi, and I. Ferreira, *Astron. Astrophys.* **454**, 409 (2006), astro-ph/0601593.
  - [16] Y. Ayaita, M. Weber, and C. Wetterich, (2009), 0905.3324.
  - [17] A. Bernui, B. Mota, M. J. Rebouças, and R. Tavakol, *Int. J. Mod. Phys.* **D16**, 411 (2007), 0706.0575.
  - [18] D. Pietrobon, P. Cabella, A. Balbi, G. de Gasperis, and N. Vittorio, (2008), 0812.2478.
  - [19] D. Pietrobon *et al.*, (2009), 0905.3702.
  - [20] A. de Oliveira-Costa and M. Tegmark, *Phys. Rev.* **D74**, 023005 (2006), astro-ph/0603369.
  - [21] L. R. Abramo, L. S. Jr., and C. A. Wuensche, *Phys. Rev.* **D74**, 083515 (2006), astro-ph/0605269.
  - [22] L.-Y. Chiang, P. Coles, P. D. Naselsky, and P. Olesen, *JCAP* **0701**, 021 (2007), astro-ph/0608421.
  - [23] A. Bernui and M. J. Rebouças, *Phys. Rev.* **D79**, 063528 (2009), 0806.3758.
  - [24] E. F. Bunn, *Phys. Rev.* **D75**, 083517 (2007), astro-ph/0607312.
  - [25] T.-P. Li, H. Liu, L.-M. Song, S.-L. Xiong, and J.-Y. Nie, (2009), 0905.0075.

- [26] P. D. Naselsky, O. V. Verkhodanov, and M. T. B. Nielsen, *Astrophys. Bull.* **63**, 216 (2008), 0707.1484.
- [27] J. P. Luminet, J. Weeks, A. Riazuelo, R. Lehoucq, and J. P. Uzan, *Nature*. **425**, 593 (2003), astro-ph/0310253.
- [28] A. Riazuelo, J. Weeks, J.-P. Uzan, R. Lehoucq, and J.-P. Luminet, *Phys. Rev.* **D69**, 103518 (2004), astro-ph/0311314.
- [29] W. S. Hipolito-Ricaldi and G. I. Gomero, *Phys. Rev.* **D72**, 103008 (2005), astro-ph/0507238.
- [30] T. Kahniashvili, G. Lavrelashvili, and B. Ratra, *Phys. Rev.* **D78**, 063012 (2008), 0807.4239.
- [31] T. Kahniashvili, Y. Maravin, and A. Kosowsky, *Phys. Rev.* **D80**, 023009 (2009), 0806.1876.
- [32] A. Bernui and W. S. Hipolito-Ricaldi, *Mon. Not. Roy. Astron. Soc.* **389**, 1453 (2008), 0807.1076.
- [33] C. Caprini, F. Finelli, D. Paoletti, and A. Riotto, *JCAP* **0906**, 021 (2009), 0903.1420.
- [34] T. R. Seshadri and K. Subramanian, *Phys. Rev. Lett.* **103**, 081303 (2009), 0902.4066.
- [35] C. Gordon, W. Hu, D. Huterer, and T. M. Crawford, *Phys. Rev.* **D72**, 103002 (2005), astro-ph/0509301.
- [36] S. Prunet, J.-P. Uzan, F. Bernardeau, and T. Brunier, *Phys. Rev.* **D71**, 083508 (2005), astro-ph/0406364.
- [37] L. Campanelli, P. Cea, and L. Tedesco, *Phys. Rev.* **D76**, 063007 (2007), 0706.3802.
- [38] L. Campanelli, (2009), 0907.3703.
- [39] T. S. Pereira, C. Pitrou, and J.-P. Uzan, *JCAP* **0709**, 006 (2007), 0707.0736.
- [40] C. Pitrou, T. S. Pereira, and J.-P. Uzan, *JCAP* **0804**, 004 (2008), 0801.3596.
- [41] A. E. Gumrukcuoglu, C. R. Contaldi, and M. Peloso, *JCAP* **0711**, 005 (2007), 0707.4179.
- [42] L. Ackerman, S. M. Carroll, and M. B. Wise, *Phys. Rev.* **D75**, 083502 (2007), astro-ph/0701357.
- [43] A. L. Erickcek, M. Kamionkowski, and S. M. Carroll, *Phys. Rev.* **D78**, 123520 (2008), 0806.0377.
- [44] A. L. Erickcek, C. M. Hirata, and M. Kamionkowski, (2009), 0907.0705.
- [45] J. F. Donoghue, K. Dutta, and A. Ross, *Phys. Rev.* **D80**, 023526 (2009), astro-ph/0703455.
- [46] Y. Shtanov and H. Pyatkovska, *Phys. Rev.* **D80**, 023521 (2009), 0904.1887.
- [47] M. Kawasaki, K. Nakayama, T. Sekiguchi, T. Suyama, and F. Takahashi, *JCAP* **0811**, 019 (2008), 0808.0009.
- [48] M. Kawasaki, K. Nakayama, T. Sekiguchi, T. Suyama, and F. Takahashi, *JCAP* **0901**, 042 (2009), 0810.0208.
- [49] C. J. Copi, D. Huterer, and G. D. Starkman, *Phys. Rev.* **D70**, 043515 (2004), astro-ph/0310511.
- [50] L. R. Abramo, A. Bernui, I. S. Ferreira, T. Villela, and C. A. Wuensche, *Phys. Rev.* **D74**, 063506 (2006), astro-ph/0604346.
- [51] G. Katz and J. Weeks, *Phys. Rev.* **D70**, 063527 (2004), astro-ph/0405631.
- [52] A. R. Pullen and M. Kamionkowski, *Phys. Rev.* **D76**, 103529 (2007), 0709.1144.
- [53] A. Hajian and T. Souradeep, *Astrophys. J.* **597**, L5 (2003), astro-ph/0308001.
- [54] A. Hajian, T. Souradeep, and N. J. Cornish, *Astrophys. J.* **618**, L63 (2004), astro-ph/0406354.
- [55] A. Hajian and T. Souradeep, (2005), astro-ph/0501001.
- [56] T. S. Pereira and L. R. Abramo, *Phys. Rev.* **D80**, 063525 (2009).
- [57] E. Hivon *et al.*, (2001), astro-ph/0105302.
- [58] A. Gut, *Probability: a graduate course*. Springer texts in statistics (Springer, 2005).
- [59] <http://lambda.gsfc.nasa.gov/>.
- [60] WMAP, N. Jarosik *et al.*, *Astrophys. J. Suppl.* **170**, 263 (2007), astro-ph/0603452.
- [61] WMAP, B. Gold *et al.*, *Astrophys. J. Suppl.* **180**, 265 (2009), 0803.0715.
- [62] WMAP, G. Hinshaw *et al.*, *Astrophys. J. Suppl.* **170**, 288 (2007), astro-ph/0603451.
- [63] J. Kim, P. Naselsky, and P. R. Christensen, *Phys. Rev.* **D77**, 103002 (2008), 0803.1394.
- [64] C.-G. Park, C. Park, and I. Gott, J. Richard, *Astrophys. J.* **660**, 959 (2007), astro-ph/0608129.
- [65] J. Delabrouille *et al.*, (2008), 0807.0773.
- [66] H. K. Eriksen, A. J. Banday, K. M. Gorski, and P. B. Lilje, *Astrophys. J.* **612**, 633 (2004), astro-ph/0403098.
- [67] <http://www.ipac.caltech.edu/2mass/>.
- [68] K. M. Gorski *et al.*, *Astrophys. J.* **622**, 759 (2005), astro-ph/0409513.